Eur. Phys. J. AP **5**, 303–310 (1999)

THE EUROPEAN PHYSICAL JOURNAL APPLIED PHYSICS

Expansion of the ablation plume created by ultraviolet laser irradiation of various target materials

B. Angleraud, J. Aubreton, and A. Catherinot[a]

Matériaux Céramiques et Traitements de Surface[b], Faculté des Sciences, 123 avenue A. Thomas, 87060 Limoges Cedex, France

Received: 9 October 1997 /Revised: 17 February 1998 / Accepted: 3 December 1998

Abstract. The plasma plume created during photoablation of various targets by an excimer KrF laser beam is studied in typical conditions of pulsed laser film deposition. For the examination of transport phenomena of ejected species, the space and time resolved evolution of the luminous plume is investigated by fast imaging as a function of laser fluence (from 7 to 200 J/cm^2) and nitrogen background pressure (from 5×10^{-3} to 500 Pa) for five different target materials (boron nitride, graphite, alumina, molybdenum, a superconducting oxide YBCO). Under "vacuum" (5×10^{-3} Pa) and for nitrogen background pressures up to 10^{-1}–1 Pa, the plume expands freely. For higher background pressures ($\geq$ 10 Pa), three successive regions above the target can be distinguished: at first the expansion is free, then the plume expands according to a shock wave-like behaviour, and lastly a drag force model correctly describes the plume shape evolution. Velocities of the luminous plasma front and of the "mass center" of the plume are determined *versus* laser fluence and background nitrogen gas pressure.

PACS. 52.70.Kz Optical (ultraviolet, visible, infrared) measurements – 52.25.Rv Emission, absorption, and scattering of visible and infrared radiation – 52.50.Jm Plasma production and heating by laser beams

1 Introduction

Pulsed laser deposition (PLD) is now well-known as a successful method for thin film deposition of various single- or multi-component materials [1,2]. However, improvement of film properties is strongly related to a sufficient understanding and a good control of phenomena involved in the photoablation process. These phenomena may be classified according to four successive steps:

- interaction between the laser beam and the target [1,3–6];
- particle desorption and formation of the Knudsen layer above the material [7–12];
- plasma plume expansion in vacuum or under background gas pressure [12–29];
- growth of a thin film on a substrate [2].

Works in this field are stimulated by the success obtained in making thin films of various materials: cubic boron nitride [30], hard carbon [31], carbon nitride [32, 33], aluminum nitride [34], and YBCO superconducting films [35].

Among the four different processes above, transport of ablated species in the plasma plume from the target to the substrate is determinant, and we are particularly concerned by its study, and by the correlation between obtained results and deposited film characteristics [36–38].

In this paper, studies concerning the transport of photoablated species in the ultraviolet (UV) laser induced plasma plume for five different target materials (boron nitride BN, graphite C, alumina Al_2O_3, molybdenum Mo, a superconducting oxide YBCO) are reported. The expansion of the photoablation plume has already been studied using similar experimental techniques for YBCO [24–26], yttrium [27], copper [28] and boron nitride [29]. This work is mainly devoted to comparison between results obtained for different materials in the same experimental conditions. The effect of the atomic mass of the ejected species on the plume expansion is particularly studied.

Experiments are performed using high-speed photography for three laser fluence values (7, 30 and 200 J/cm^2). Since PLD is frequently performed under background gas pressure, the influence of this deposition parameter on the plume expansion is particularly investigated (from 5×10^{-3} to 500 Pa).

2 Experimental set-up

The experimental apparatus for fast imaging is schematically shown in Figure 1. The UV laser source used is a pulsed excimer laser (Lambda Physik EMG 150) operating at 248 nm (KrF). Pulse duration is of 20 ns and energy per pulse is in the range 150–220 mJ. The laser beam is focused onto the target material using a fused silica lens (UV grade) with an incidence of 45° relative to the

[a] e-mail: catherinot@unilim.fr

[b] UPRESA 6015 CNRS

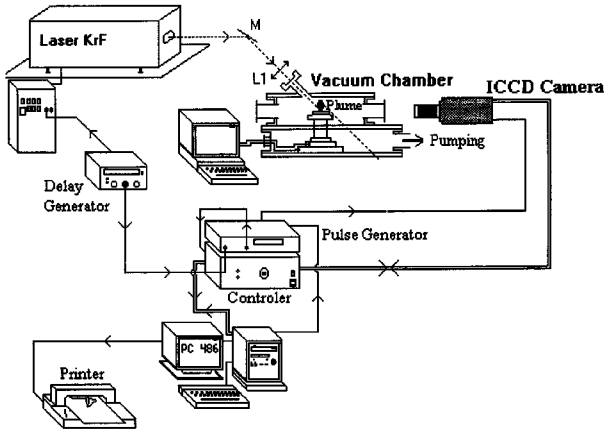

Fig. 1. Experimental set-up.

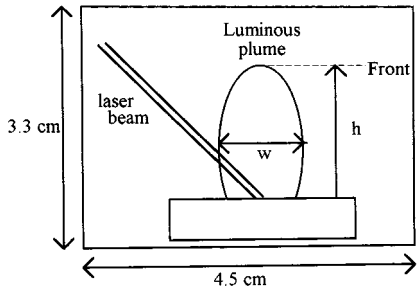

Fig. 2. Schematic representation of the region observed by the ICCD camera; h and w are respectively the height of the luminous front and the width of the plume. The laser beam comes from the left with an incidence of 45°.

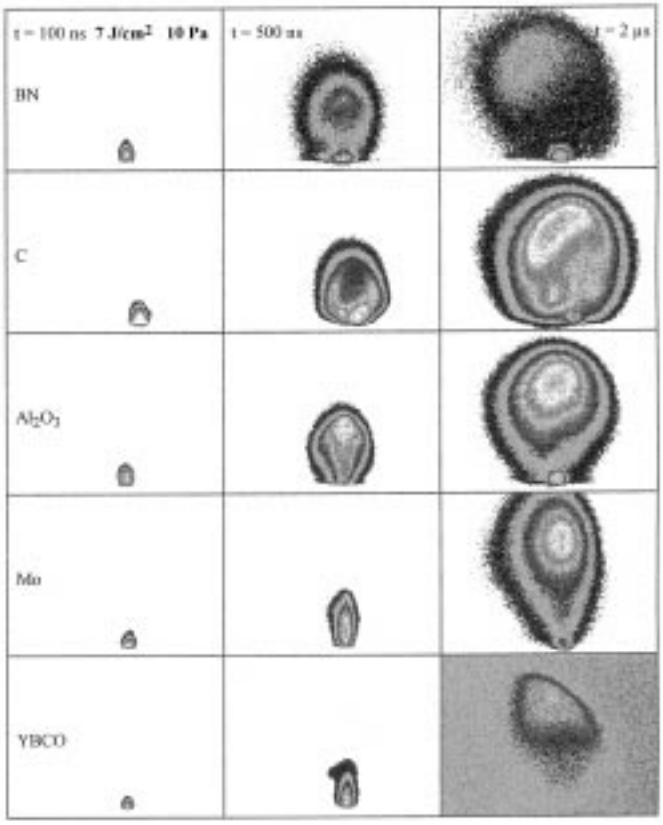

Fig. 3. Images of the plumes created above the five targets, performed at 7 J/cm^2, 10 Pa (N_2) (size: 3.3×4.5 cm^2 (height × width)) for three delays t after the beginning of the laser pulse (duration 20 ns). The target is at the bottom of each image.

normal at the target surface. Laser fluence (energy per unit area) is deduced from impact area and pulse energy measurements. Taking into account losses due to the lens and the different mirrors and windows, laser fluence can be varied from 1 to 200 J/cm^2 by varying laser pulse energy, with a mean measurement uncertainty of 20% and a reproducibility better than 5%.

The target is located in a stainless-steel vacuum cell equipped with fused silica windows, and is moved between each laser pulse to avoid excessive local digging.

High-speed photography of the plume is performed using a gated, intensified coupled charge device (ICCD) camera (576 G/RB-E Princeton Instruments, 576×384 pixels) equipped with a 105 mm Nikon telephoto lens (spectral range: 350–800 nm). The camera, located at about 50 cm from the plasma, provides two-dimensional intensity distribution measurements of the luminous plume (integrated over the spectral range). The observation plane is parallel to those defined by the laser beam which comes from the left of the images reported in this paper, and the direction normal to the surface target. As shown in Figure 2, the size of the observed region is $3.3 \times 4.5 \approx 15$ cm^2 (height × width). The exposure time (duration of intensification of the CCD) is 10 ns and each image is obtained from a single laser pulse. A computer controls the storage of the images which are processed by software.

Images performed at various delays t (40 ns–100 μs) after the beginning of the laser pulse, yield to luminous plasma plume time evolution.

The incidence of a background gas pressure (from 5×10^{-3} up to several hundreds of Pa) on the plasma expansion, is investigated by injecting nitrogen in the chamber during experiments.

3 Results and discussion

3.1 General sight of the luminous plumes created above the different targets

3.1.1 Expansion

Images of plumes obtained with the five targets, are reported in Figure 3 for three delays t after the beginning of the laser pulse: 100, 500 and 2000 ns. The laser fluence is 7 J/cm^2 and the background nitrogen pressure is 10 Pa. We observe that the plume shapes are similar for the five different targets: the material is ejected above the surface as a luminous cloud the size of which increases with time. The grey-scale palette of the pictures is representative of the light intensity measured by the camera. So we can distinguish a very luminous plume core (white and grey

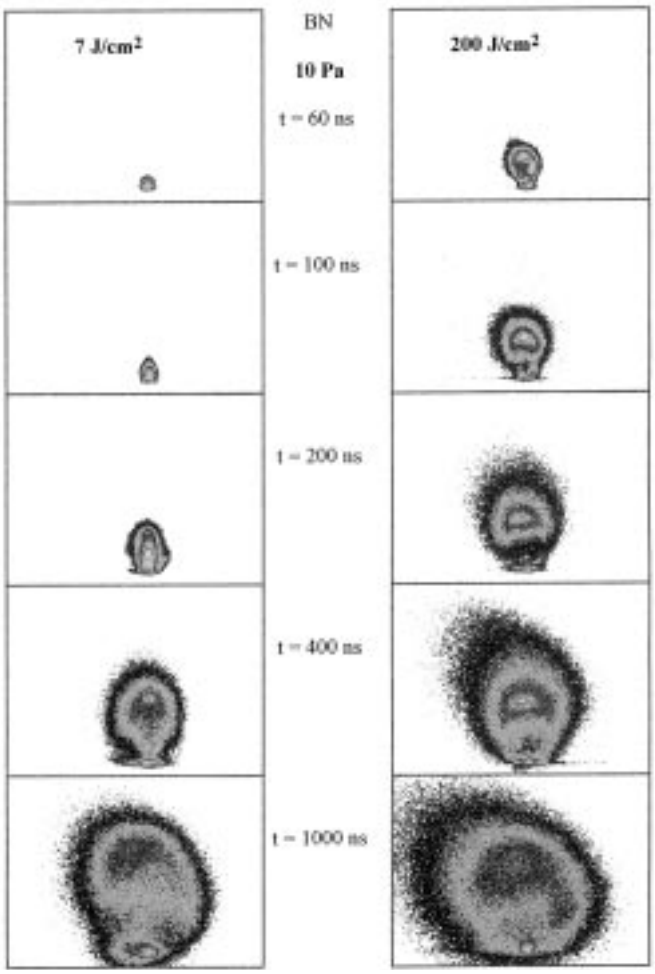

Fig. 4. Evolution of the plume created above a BN target, performed at 10 Pa (N_2) as a function of the laser fluence: 7 and 200 J/cm^2 (delays t from 60 to 1000 ns).

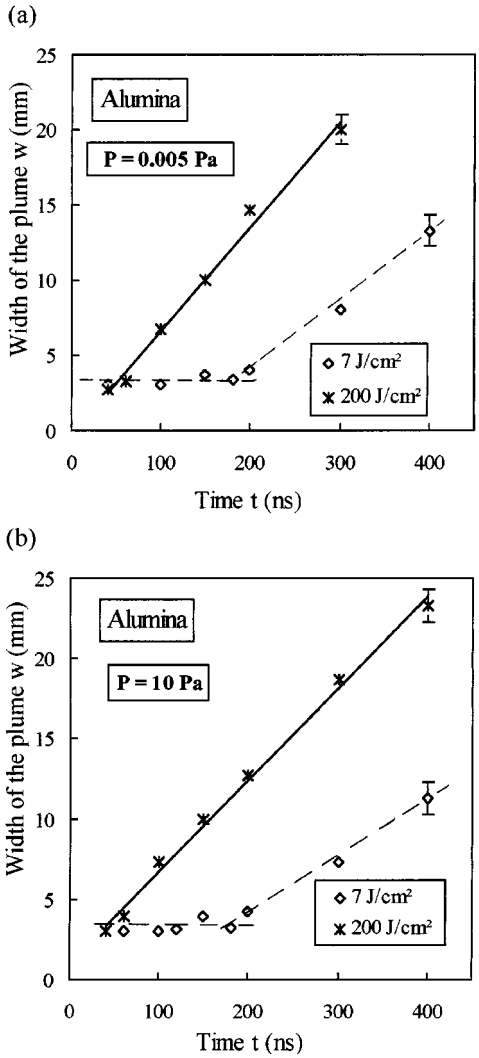

Fig. 5. Evolution of width w (mm) of the plume (alumina target) with delay time t (ns) and with laser fluence (7 and 200 J/cm^2): (a) at 5×10^{-3} Pa (vacuum); (b) at 10 Pa (N_2 gas).

regions) preceded by a much less luminous front (black outline).

In Figure 4, images of the plume created above the boron nitride target are presented for two laser fluences: 7 and 200 J/cm^2 (10 Pa). They are reported for several delays t after the beginning of the laser pulse: 40 ns up to 1 μs. The height h reached at time t by the luminous plume (upper leading edge in Figure 2) increases with laser fluence.

It is interesting to determine the type of expansion followed by the plume: one or three-dimensional. So, in Figure 5, the width w (dimension parallel to the target surface defined in Fig. 2) of the luminous plume created above the alumina target is plotted *versus* time for two background gas pressures (5×10^{-3} and 10 Pa) and for two laser fluences (7 and 200 J/cm^2). At 7 J/cm^2 and whatever the background gas pressure, w remains constant during $\approx$ 200 ns and then begins to increase. As h increases with time since the beginning of observation, we can conclude that the material is ejected in a direction normal to the target surface (expansion with preferential direction), then the plume expands in the three directions of the space. So, the expansion is at first one-dimensional (1D) then becomes three-dimensional (3D) for $t > 200$ ns. This has been previously observed for copper targets [28, 39]. This phenomenon is attributed to the fact that the initial gradients of density and pressure (within the plasma plume) in the direction normal to the target surface are much larger than those in the parallel directions [14–17, 39]. This can be explained by the large initial differences between the dimensions of the laser spot on the target surface ($\approx 10^{-2}$ cm measured by optical microscopy) and the depth of material removal of the laser beam in the target ($d_p < 10^{-5}$ cm determined using a profilometer).

At higher laser fluences (30 and 200 J/cm^2), as shown in Figure 4 (200 J/cm^2), the expansion is quite immediately 3D (no preferential direction is observed). This observation can be explained by simple geometrical considerations. The difference between the depth of material

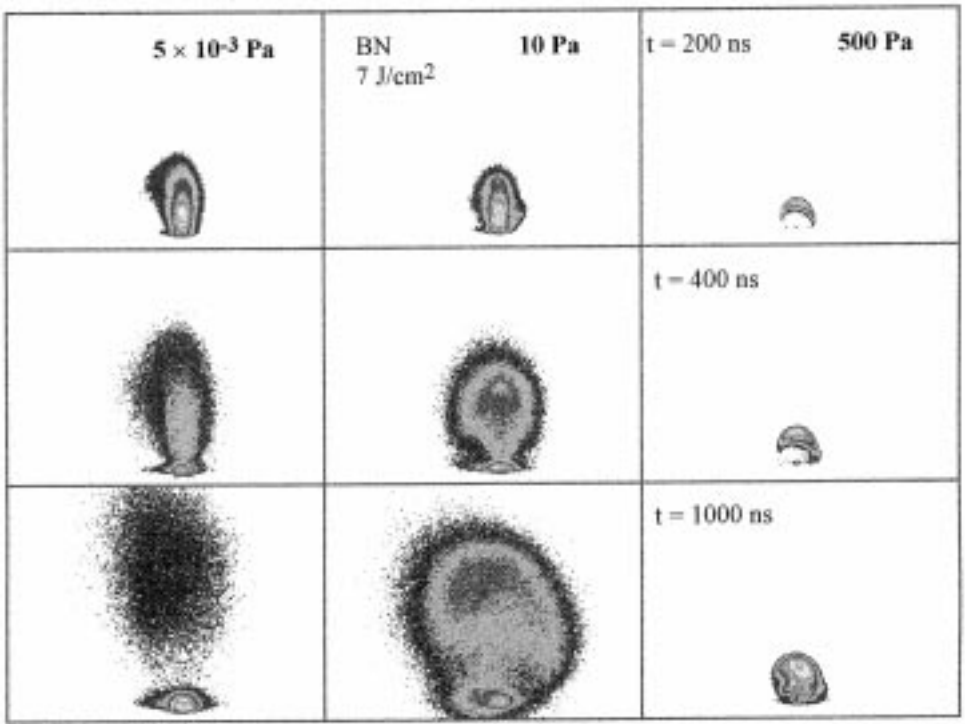

Fig. 6. Evolution of the plume created above a BN target, performed at 7 J/cm^2 as a function of pressure in the cell: under vacuum (5×10^{-3} Pa), at 10 and 500 Pa (N_2) (delays t: 200, 400, 1000 ns).

removal (which increases with increasing the laser fluence, $d_p \approx 10^{-4}$–10^{-3} cm at 200 J/cm^2) and the dimensions of the laser spot ($\approx 10^{-2}$ cm), diminishes. Hence the initial gradients of density in the three directions tends to equilibrate leading to a 3D expansion.

We can conclude that at low fluences (several J/cm^2) the expansion of the plasma is firstly 1D, then it becomes 3D at $\approx$ 200 ns. When increasing the fluence, the one-dimensional step is shortened and tends to disappear at high fluences (30 and 200 J/cm^2).

3.1.2 Effect of the background gas pressure (N_2)

In Figure 6, images of the plume are reported for a BN target. They are performed at 7 J/cm^2 under vacuum (residual pressure: 5×10^{-3} Pa) and at two nitrogen pressures (10 and 500 Pa) for three delays: 200, 400 and 1000 ns. We immediately notice an important evolution of the plasma plume shape. To quantify the observed results, we define h as the height reached by the leading edge of the luminous plasma plume (front) (Fig. 2). The height h is plotted in Figures 7 and 8 *versus* time for two pressures (5×10^{-3} and 10 Pa). The height reached by the front at a fixed time decreases when the pressure increases. This effect is particularly evident for pressures above 10^{-1}–1 Pa, as shown in Figure 9. The measurements have been performed with a BN target, at 13 J/cm^2 for a delay of 200 ns. This phenomenon is attributed to the collisions between nitrogen background gas molecules and species ejected from the target, and may be correlated to the value of the mean free path λ of ejected species in the background gas. The value of λ is several tens of cm under vacuum and becomes

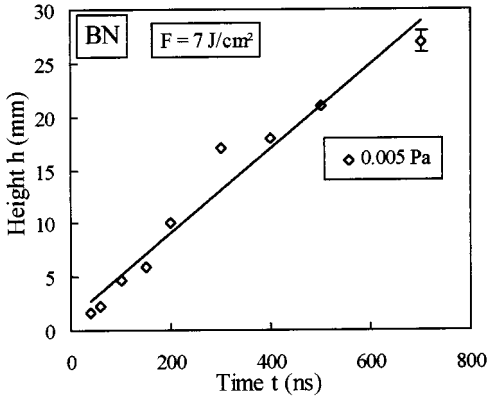

Fig. 7. Evolution of height h (mm) reached by the front (BN target) with delay time t (ns) at 7 J/cm^2 under vacuum: free motion.

of same order of magnitude as the plume dimensions (several centimeters) when the pressure reaches 10^{-1} Pa.

A more detailed examination of Figures 7 and 8 leads to the following results.

- Under vacuum ($P < 10^{-1}$ Pa): the position h of the front above the target follows a linear law *versus* time t (Fig. 7):

$$h(t) = a_0 t. \quad (1)$$

As expected, this indicates a free expansion of the plume, without any collision with background gas molecules. For delays larger than 1 μs, the luminous plume leaves the observed region. Particularly, when a PLD experiment is carried out in such conditions, ejected

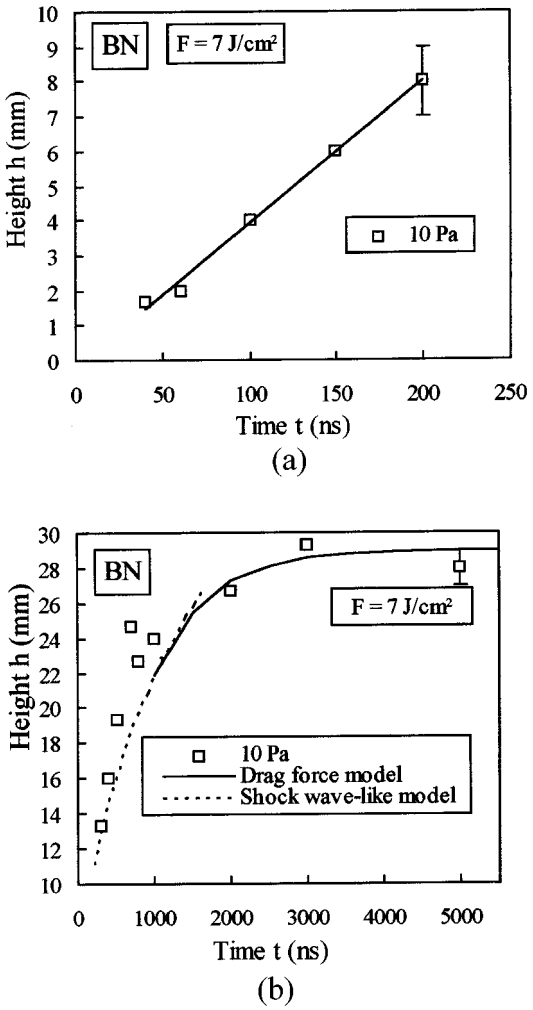

Fig. 8. Evolution of height h (mm) reached by the front (BN target) with delay time t (ns) at 7 J/cm^2 at 10 Pa (N_2): (a) h up to 1 cm: free motion; (b) $h > 1$ cm: dotted curve = the shock wave model fit; full curve = the drag force model fit.

species reach the substrate, located typically at a distance of $\approx$ 3–4 cm in front to the target, without significant loss of kinetic energy.

- For $P > 10^{-1}$ Pa: three successive regions above the target may be distinguished (Fig. 8: 10 Pa):
  - for $h < 1$ cm (Fig. 8a). The front of the plasma follows a similar regime of expansion as under vacuum described by (1). However the slope of the linear function $h(t)$ depends on the background pressure;
  - for 1 cm $< h <$ 2.5 cm (Fig. 8b), the front is slowed down. The experimental results are typically described as follows:

$$h(t) = a_0 t^{a_1}. \tag{2}$$

Mean square fit of experimental data leads to a value of 0.40 ± 0.02 for the exponent a_1. This value is in good agreement with reference [40] ($a_1 = 2/5$) describing the propagation of a spherical shock wave front through a background gas (density ρ_0) caused by the sudden release (in a small volume) of an energy E in an explosion, namely:

$$h = \zeta_0 \left(\frac{E}{\rho_0}\right)^{\frac{1}{5}} t^{\frac{2}{5}} \tag{3}$$

where ζ_0 is a dimensionless quantity. In our case E is the laser incident energy, ρ_0 is the density of the background nitrogen gas in the cell. This model is only valid when two conditions are fulfilled. First, the initial volume, where the incident energy is dissipated, has to be very small in comparison with the dimensions of the plume. Hence the energy release can be assumed to occur at a point. Second, the ambient pressure has to be neglected in comparison with the pressure in the plume behind the front. This is equivalent to neglecting the initial internal energy of the gas which has been set in motion in comparison with the explosion energy E. These conditions define a region where the shock wave model may be applied to describe the propagation of the front. In our case, this region is approximately between 1 and 2.5 cm above the target surface at 10 Pa (at 500 Pa, these values are 0.5 and 1 cm respectively);

  - for $h >$ 2.5 cm. The plasma has expanded in the three dimensions of the space, so its volume has increased. Hence the pressure within the plume has decreased and tends to equilibrate with the background pressure. As shown in Figure 8b, the leading edge is drastically slowed down and reaches a maximum value $h_{\rm lim}$ above the target surface. In this region, the evolution of the plume is well-described by a drag force model [24]:

$$h(t) = h_{\rm lim}\left[1 - \exp\left(-\beta t\right)\right]. \tag{4}$$

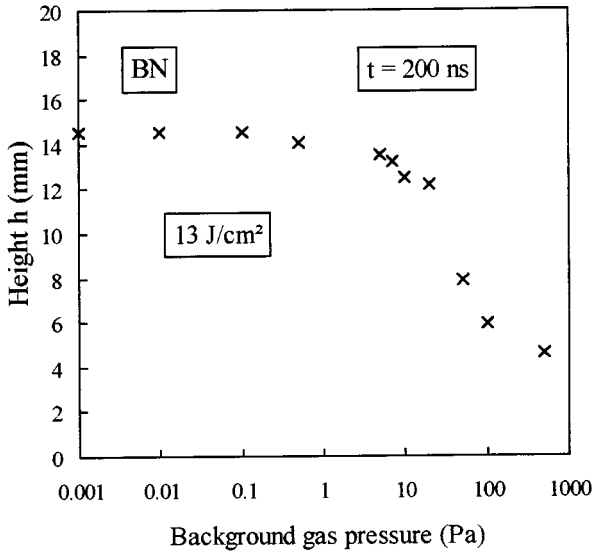

Fig. 9. Height h reached by the luminous front at $t = 200$ ns above a BN target (13 J/cm^2) as a function of pressure in the cell: from residual background pressure up to 500 Pa (N_2).

In equation (4), β is the slowing coefficient and $h_{\lim}$ is the maximum distance from the target reached by the plume front. As shown in Figure 8b, $h_{\lim}$ is about 3 cm at 10 Pa in the case of the BN target and $h_{\lim}$ is found to be 2 cm at 500 Pa.

For the five target materials, we find that the description in three spatial regions, as defined above with the same values of h, appears to be independent of the laser fluence and of the target material. Though these spatial regions are the same whatever the target material, they correspond to different temporal ranges in the plume evolution. This fact is due to the differences of ejected particle velocities which depend on laser fluence and target material mass, as discussed in Section 3.1.1.

The results presented above, concern the motion of the fastest species. To investigate the transport of the global plume, we have studied the motion of the "mass center" (CM) of the luminous plume. Its position is determined using image processing software, that calculates the pondered intensity of the "mass center" of the plume image. The results show that the CM follows the same evolution as the front. Namely, under vacuum, the expansion is free, and for pressures $> 10^{-1}$ Pa, we find again the three spatial regions: free expansion, then shock wave – like expansion and finally a slowing down governed by drag forces. As the front, these three spatial regions are independent of laser fluence and target material.

3.2 Quantitative study of the plume expansion

As previously quoted, the ICCD camera detects only the emission of the plume in the visible spectral range (350–800 nm). The emitting species detected, for the different target materials under study, are reported in Table 1. We should notice that the emitted light intensities of the diatomic species are very weak in comparison with the atomic ones. Consequently, the results, deduced from experimental measurements, are related to atomic species only.

Although the following results are concerning only the light emitting species of the plume, they are roughly representative of all species. For example, the velocities of carbon ions measured using a Faraday cup [31] are in agreement with those deduced by ICCD imaging. Moreover, one of the main advantage of optical emission spectroscopy using ICCD camera, is that this diagnostic technique gives an instantaneous undisturbed view of the whole luminous plume at any step of the expansion (contrary to ion detection or mass spectrometry).

3.2.1 Velocity and kinetic energy of the fastest species

In Figure 4, images performed for a BN target with a background nitrogen pressure of 10 Pa, are reported for two fluences 7 and 200 J/cm^2. The height h reached by the front of the luminous plume increases with the fluence as a consequence of the increase of the plume velocity and hence of the ejected species. In Table 2, velocities and kinetic energies of ejected species are reported for three background pressures (5×10^{-3}, 10 Pa and 500 Pa) and for three laser fluences (7, 30 and 200 J/cm^2). Velocities are deduced from the slope of the curves $h(t)$ in the free expansion region, through the relation (1). Kinetic energies are calculated using the mean atomic weight M of the ejected atomic species reported in Table 1, hence M is 12.5 g for BN, 12 g for graphite, 27 g for alumina, 96 g for molybdenum, 97 g for YBCO.

Table 1. Emitting species detected in the plume by optical emission spectroscopy above the five targets.

Target	Emitting species	References
boron nitride	B, B^+, B^{++}, N^+	[15,29,36]
graphite	C^+, C^{++2}, C_2,	[35]
alumina	Al, Al^+, AlO	[15]
molybdenum	Mo, Mo^+	[15]
YBCO	Y, Ba, Cu, Y^+, Ba^+, Cu^+, YO, BaO, CuO	[37]

Table 2. Velocity V (km/s) and kinetic energy E_c (eV) of the front *versus* laser fluence and background gas pressure. For the calculation of E_c, only atomic species are taken into account.

5×10^{-3} Pa		B, N	C	Al	Mo	YBC
7 J/cm^2	V	40	44	31	15	15
	E_c	91	120	134	110	113
30 J/cm^2	V	52	53	36	21	21
	E_c	175	175	182	220	222
200 J/cm^2	V	88	88	60	28	29
	E_c	500	440	500	390	420
10 Pa						
7 J/cm^2	V	30	30	22	14	14
	E_c	58	56	68	98	99
30 J/cm^2	V	36	32	29	19	20
	E_c	84	64	118	180	200
200 J/cm^2	V	60	55	45	23	23
	E_c	233	190	280	263	266
500 Pa						
7 J/cm^2	V	6.4	-	-	-	-
	E_c	2.7	-	-	-	-

(mean error on the velocity: 10%; on the kinetic energy: 20%)

Under vacuum (5×10^{-3} Pa)

At low laser fluences (7 J/cm^2), the measured velocities vary between 15 km/s for the "heavy" species, ejected from the molybdenum Mo and YBCO targets. They are about 40–45 km/s for the "light" ones, ejected from the boron nitride and graphite targets. The kinetic energy is typically about 100 eV for all species.

At medium fluence (30 J/cm^2), velocities are about 20 and 50 km/s for the "heavy" and "light" species respectively, and the mean kinetic energy is about 200 eV.

At high fluence (200 J/cm^2), velocities are between 30 km/s for the "heavy" species and 90 km/s for the "light" ones and the mean kinetic energy is about 450 eV. It appears that the increase of the laser fluence from 7 to 200 J/cm^2 leads to an important increase of velocities ($\times 2$) and of kinetic energies ($\times 4$) (Tab. 2). This result gives an useful guide to estimate the kinetic energy of bombarding particles in PLD processes and consequently their influence on surface diffusion phenomena, known to play an important role in film growth. Note that the laser fluence values in this study correspond to the range currently used for film deposition.

Under a background gas pressure (nitrogen)

As shown in Table 2, we observe a decrease of velocities and kinetic energies of the ejected species when the pressure increases. Whatever the laser fluence, this decrease is more important for "light" species than for heavy ones. This result is in agreement with the values of the transfer coefficient α of kinetic energy in an elastic collision between a particle of mass m_1, belonging to the plume, and a background nitrogen molecule of mass m_2:

$$\alpha = 2m_1m_2/(m_1 + m_2)^2. \quad (5)$$

To validate the shock wave model, presented in Section 3.1.2, for a 10^{-1} Pa background pressure, the velocity ratios measured at different laser fluences have been compared with ratios of the respective laser fluences at 10 Pa. As expected, the measured front velocity of the plume is found to vary like $F^{1/5}$ (F: laser fluence). This is in agreement with the shock wave front velocity calculated by differentiating the relation (3) with respect to time (dependence with $E^{1/5}$). Hence, the expansion may be assimilated to a blowing up from a point source [40].

At 500 Pa, the plume is confined very near the target surface and velocities and kinetic energies decrease drastically. For example, for a BN target, the front velocity calculated in the free expansion step is 6.4 km/s meaning a kinetic energy of 2.7 eV. For large delays, the expansion is well-described by equation (4) with $h_{\lim} = 2$ cm, the maximum distance from the target reached by the ejected particles.

These results have important consequences on film deposition, particularly in the PLD process under a reactive atmosphere. Indeed, target-substrate distance must be chosen as a function of ambient pressure and great care has to be taken of the decrease of particle kinetic energy with increasing pressure.

3.2.2 Velocity and kinetic energy of the "center of mass" CM

In Table 3, velocities and kinetic energies of the CM at 5×10^{-3} and 10 Pa, for 7 and 200 J/cm^2 are reported.

Table 3. Velocity V (km/s) and kinetic energy E_c (eV) of "mass center" *versus* laser fluence and background gas pressure. For the calculation of E_c, only atomic species are taken into account.

5×10^{-3} Pa		B, N	C	Al	Mo	YBC
7 J/cm^2	V	22	25	16	8	6
	E_c	30	36	36	32	18
200 J/cm^2	V	40	44	30	13	12
	E_c	100	120	126	84	72.5
10 Pa						
7 J/cm^2	V	17	13	14	7	6
	E_c	19	10	27	24	18
200 J/cm^2	V	30	25	28	12	11
	E_c	50	40	110	72	61

(mean error on the velocity: 10%; on the kinetic energy: 20%)

The values are lower, by a factor of two for velocities and a factor of four for kinetic energies, in comparison with values given in Table 2. The plasma plume is like a luminous cloud whose time evolution is slow in comparison with the displacement of its front.

Under vacuum, the CM kinetic energy decreases when the mass of the species increases whatever fluence (on the contrary, the kinetic energy is constant for the fastest species, as reported in Sect. 3.2.1). This phenomenon may be attributed to the collisions between species within the core of the plume. These collisions lead to a loss of energy, that is greater for heavy species than for light ones.

At 10 Pa, we observe for the CM the same behaviour as for the species of the front, but with lower velocities and kinetic energies.

From all these results, in a PLD process we can consider that the growing film is first bombarded by the fastest species belonging to the plume front. Then this bombardment is followed by the arrival of the plume core with relatively low velocity and energy but containing a high particle density.

4 Conclusion

We have reported the study of the expansion of the UV laser induced – luminous plasma plume created above different target materials (BN, C, Al_2O_3, Mo, YBCO), under typical conditions of pulsed laser deposition. High-speed photography of the plume has been performed whilst varying the laser fluence (7, 30 and 200 J/cm^2) and the background gas pressure in the cell from vacuum to 500 Pa:

- at low fluence (≈ 7 J/cm^2), the expansion is 1D up to a delay of about 200 ns and then becomes 3D;
- at high fluence (≈ 200 J/cm^2), the 1D step is drastically shortened and the 3D step is directly observed.

In vacuum, the transport motion of the ejected matter is free, whereas at 10^{-1} Pa, three successive regions above

the target surface can be distinguished, with three different plume expansion laws: free expansion, shock wave expansion similar to a blowing up from a point source, followed by a slowing regime dominated by drag forces. Moreover, these expansion regimes do not depend on the atomic mass of the ejected species as the three successive regions are the same whatever the target material.

Velocities and kinetic energies of the ejected particles have been measured and calculated respectively for the front and for the CM. In vacuum the kinetic energy depends only on the laser fluence. In a background gas with a pressure above 10^{-1} Pa, the kinetic energy of the ejected species depends on their atomic mass due to different collision loss coefficients. Core plume velocity and kinetic energy are lower than those of the front, the values are divided by 2 and 4 respectively.

In summary, the plume expansion is greatly influenced by the laser fluence and the background gas pressure. The qualitative results, concerning the plume expansion, are very similar for the five target materials, whereas evolutions of velocity and kinetic energy of ejected species (quantitative results) are mass dependent.

This work was partially supported by DRET contract No. 92-067.

References

1. K.L. Saenger, Part I: Proc. Adv. Mater. **2**, 1 (1993); Part II: *ibid.* **3**, 63 (1993).
2. D.B. Chrisey, G.H. Hubler, *Pulsed Laser Deposition of Thin Films* (Wiley Interscience Publication, J. Wiley & Sons Inc., 1994).
3. M. von Allmen, *Laser Beam Interactions With Materials* (Springer Series in Material Science, 1987).
4. I.W. Boyd, *Laser Processing of Thin Films and Microstructures* (Springer Series in material Science, 1987).
5. A.M. Prokhorov, V.I. Konov, I. Ursu, I.N. Mihailescu, *Laser Heating of Metals* (Adam Hilger Series on Optics and Optoelectronics, 1990).
6. *Surface Processing and Laser Assisted Chemistry Proceeding of Symposium E*, edited by I.W. Boyd, E. Fogarassy, M. Stuke (E-MRS Spring Conference, North-Holland, 1990).
7. S.I. Anisimov, Sov. Phys. JETP **27**, 182 (1968) .
8. Ch.J. Knight, AIAA J. **17**, 519 (1979).
9. R. Kelly, R.W. Dreyfus, Surf. Sci. **198**, 263 (1988); Nucl. Instr. Meth. Phys. Res. B **32**, 341 (1988).
10. I. Noorbatcha, R. Lucchese, Y. Zeiri, J. Chem. Phys. **89**, 5251 (1988).
11. R. Kelly, J. Chem. Phys. **92**, 5047 (1990).
12. R. Kelly, A. Miotello, B. Braren, A. Gupta, K. Casey, Nucl. Instr. Meth. Phys. Res. B **65**, 187 (1992).
13. S.K. Godunov, A.V. Zabrodin, G.P. Prokopov, Z.h. Vych, Mat. **1**, 1020 (1961).
14. J. Dawson, P. Kaw, B. Green, Phys. Fluids **12**, 875 (1969).
15. R.K. Singh, J. Narayan, Phys. Rev. B **41**, 8843 (1990).
16. R.K. Singh, O.W Holland, J. Narayan, J. Appl. Phys. **68**, 233 (1990).
17. J. Hermann, Ph.D. thesis, University of Orléans, France, 1991.
18. M. Aden, E. Beyer, G. Herziger, H. Kunze, J. Phys. D **25**, 57 (1992).
19. D.B. Geohegan, Thin Solid Films **220**, 138 (1992).
20. R.W. Dreyfus, C. Phipps, A. Vertes, *Laser Ablation: mechanisms and applications II*, edited by J.C. Miller, D.B. Geohegan, Knoxville TN, AIP Conf. Proc. **275**, 285 (1993).
21. E.Y. Lo, W.T. Lauglin, E.R. Pugh, *Laser Ablation: mechanisms and applications II*, edited by J.C. Miller, D.B. Geohegan, Knoxville TN, AIP Conf. Proc. **275**, 291 (1993).
22. M. Aden, E.W. Kreutz, A. Voss, J. Phys. D **26**, 1545 (1993).
23. D. Fried, G.P. Reck, T. Kushida, G. Kim, E.W. Rothe, Appl. Spectr. **47**, 1046 (1993).
24. W. Pietch, Ph.D. thesis, University of Orléans, France, 1994.
25. B. Angleraud, Ph.D. thesis, University of Limoges, France, 1995.
26. S. Proyer, E. Stangl, Appl. Phys. A **60**, 573 (1995).
27. D.B. Geohegan, A.A. Puretzky, Appl. Phys. Lett. **67**, 197 (1995).
28. W. Pietsch, B. Dubreuil, A. Briand, Appl. Phys. B **61**, 267 (1995).
29. B. Angleraud, C. Girault, C. Champeaux, F. Garrelie, C. Germain, A. Catherinot, Appl. Surf. Sci. **96-98**, 117 (1996).
30. P.B. Mirkarimi, K.F. McCarty, D.L. Medlin, W.G. Wolfer, T.A. Friedmann, E.J. Klaus, G.F. Cardinale, D.G. Howitt, J. Mat. Res. **9**, 2925 (1994).
31. C. Germain, C. Girault, J. Aubreton, A. Catherinot, S. Bec, A. Tonck, Diamond Rel. Mat. **4**, 309 (1995).
32. Z.M. Ren, Y.C. Du, Y.X. Qiu, J.D. Nu, Z.F. Ying, X.X. Xiong, F.M. Li, Phys. Rev. B: Cond. Mat. **51**, 5274 (1995).
33. Z.J. Zhang, S. Fan, C.M. Lieber, Appl. Phys. Lett. **66**, 3582 (1995).
34. W.T. Lin, L.C. Meng, G.J. Chen, H.S. Liu, Appl. Phys. Lett. **66**, 2066 (1995).
35. C. Champeaux, P. Marchet, J. Aubreton, J.P. Mercurio, A. Catherinot, Appl. Surf. Sci. **69**, 335 (1993).
36. C. Girault, D. Damiani, C. Champeaux, P. Marchet, C. Germain, J.P. Mercurio, J. Aubreton, A. Catherinot, Appl. Surf. Sci. **46**, 78 (1990).
37. B. Angleraud, C. Champeaux, C. Girault, J. Aubreton, A. Catherinot, Escampig 94 (XII) Eindhoven ed. MCM van de Sanden Eur. Phys. Society august the 23 - 26th (1994) 304.
38. A. Catherinot, A. Angleraud, J. Aubreton, C. Champeaux, C. Germain, C. Girault, *Surface Treatment and Film Deposition*, NATO ASI series Profs, edited by O. Conde, J. Mazunder, R. Vilar (Kluwer Academic publishers Lisbon Portugal 1995), Chap. Laser Processing.
39. J.C.S. Kools, T.S. Baller, S.T. Dezwart, J. Dieleman, J. Appl. Phys. **71**, 4547 (1992).
40. Ya.B. Zel'dovich, Yu. Raizer, *Physics of shock-waves and high-temperature phenomena* (Academic Press New-York and London, 1966), p. 94.